Eur Biophys J (2010) 39:947–957
DOI 10.1007/s00249-009-0461-x

ORIGINAL PAPER

Understanding biological dynamics: following cells and molecules to track functions and mechanisms

A. Palamidessi · I. Testa · E. Frittoli · S. Barozzi · M. Garrè · D. Mazza · P. P. Di Fiore · A. Diaspro · G. Scita · Mario Faretta

Received: 29 January 2009 / Revised: 8 April 2009 / Accepted: 20 April 2009 / Published online: 20 May 2009

Abstract The dissection of the molecular circuitries at the base of cell life and the identification of their abnormal transformation during carcinogenesis rely on the characterization of biological phenotypes generated by targeted overexpression or deletion of gene products through genetic manipulation. Fluorescence microscopy provides a wide variety of tools to monitor cell life with minimal perturbations. The observation of living cells requires the selection of a correct balance between temporal, spatial and "statistical" resolution according to the process to be analyzed. In the following paper ad hoc developed optical tools for dynamical tracking from cellular to molecular resolution will be presented. Particular emphasis will be devoted to discuss how to exploit light–matter interaction to selectively target specific molecular species, understanding the relationships between their intracellular compartmentalization and function.

Keywords Fluorescence microscopy · Cell tracking · Fluorescence recovery after photobleaching · Photoactivation · Two-photon microscopy

Proceedings of the XIX Congress of the Italian Society of Pure and Applied Biophysics (SIBPA), Rome, September 2008.

A. Palamidessi and I. Testa contributed equally to this work.

S. Barozzi · M. Faretta
Dipartimento di Oncologia Sperimentale,
IEO, Istituto Europeo di Oncologia, 20141 Milan, Italy

I. Testa · D. Mazza · A. Diaspro
LAMBS-MicroScoBio, Department of Physics,
University of Genoa, 16146 Genoa, Italy

A. Palamidessi · E. Frittoli · M. Garrè · P. P. Di Fiore · A. Diaspro · G. Scita
IFOM, Fondazione Istituto FIRC di Oncologia Molecolare,
20139 Milan, Italy

S. Barozzi · M. Garrè
Consortium for Genomic Technologies,
COGENTECH, 20139 Milan, Italy

P. P. Di Fiore · G. Scita
Dipartimento di Medicina, Chirurgia ed Odontoiatria,
Universita′ degli Studi di Milano, 20122 Milan, Italy

M. Faretta (✉)
Department of Experimental Oncology, IEO,
IFOM-IEO-Campus, via Adamello 16, 20139 Milan, Italy
e-mail: mario.faretta@ifom-ieo-campus.it

Introduction

The completion of the human genome sequencing project put a milestone in the evolution of biomedical research, delivering us information about 20,000–25,000 gene sequences present in our DNA. As a result the key question "What does a gene do?" was exponentially multiplied, requiring new experimental and technological approaches to find an answer for all the coded gene products presently known. Optical microscopy, and in particular fluorescence microscopy, still remains one of the most important tools for life science thanks to its incomparable ability to observe living cells with good temporal and spatial resolution and excellent sensitivity. Moreover the continuous technological evolution continuously provides new solutions for cell biology investigation. Stimulated emission depletion (STED) microscopy, 4Pi microscopy, photoactivated localization microscopy (PALM), and stochastic optical reconstruction microscopy (STORM) overcame the 200-nm diffraction barrier and pushed spatial resolution towards the

limit of electron microscopy, giving rise to "far-field nanoscopy" (Hell 2007, 2009; Lippincott-Schwartz and Manley 2009). In parallel, the slow acquisition time typical of confocal microscopy was dramatically ameliorated by parallelization in spinning disk microscopy or in other new raster scanning techniques (Bansal et al. 2006; Graf et al. 2005; Kurtz et al. 2006; Maddox et al. 2003; Reddy and Saggau 2005; Saggau 2006; Wolleschensky et al. 2006). The evolution in the detection technology maintained optimal signal-to-noise ratio even for the acquisition of very fast processes.

Similarly to physics, where the Heisenberg uncertainty principle stated the limit in experimental precision for determination of the spatial position and velocity of a particle, fluorescence microscopy experienced intrinsic limitations. The increment in spatial resolution causes a reduction in the acquisition speed, and consequently temporal resolution, and a diminished number of collected photons, thus impacting on the signal-to-noise ratio. Consequently microscopy sciences have to play on a triangular playground having as vertexes spatial resolution, temporal resolution, and signal-to-noise ratio: increasing the precision for each parameter inevitably implies operating far from the maximization of the others.

The sequencing of the human genome pushed for the addition of an additional vertex, namely the throughput or "statistical resolution" of the analysis. An increased throughput is required for the rapid acquisition of large numbers of heterogeneous events originated from phenotype screening of DNA or RNA constructs. At the same time, a large amount of data is mandatory to validate observations on targeted cell populations with low representation frequency as is the case of stem cells. The analysis of complex samples such as tissue biopsies still demands increased data collection. In all the aforementioned cases, the amount of information retrieved can and must be optimized by a high-content analysis which maximizes the number of simultaneously measured parameters.

The visualization and tracking of cells and the reconstruction of intracellular structures and/or molecular trajectories have always been main challenges for live cell imaging. The reconstruction of spatial trajectories drawn by target cells in unbiased conditions (random cell migration) or in presence of specific stimuli (presence of chemoattractants, wound healing assays) frequently relies on the expression of fluorescence markers to identify cells of interest and to allow semi-automatic tracking. However, both data acquisition and analysis in cell mobility assays are still limited in their statistical significance due to the relatively low number of measurements.

Even if the steady-state expression of fluorescent markers is an efficient tool for the reconstruction of dynamic maps at low resolution, it could sometimes be limiting when applied to the study of molecular mobility in cell compartments. The tracking of single molecules under low-copy-number expression conditions has been successfully employed for in vivo intracellular quantification using fluorescent proteins (Leake et al. 2006; Ulbrich and Isacoff 2007). However, molecular crowding makes the reconstruction of single object trajectories very difficult. To bypass this bottleneck, new techniques have been developed. Fluorescence recovery after photobleaching (FRAP) and photoactivation employed the local manipulation of the photophysical properties of fluorescent molecules to tag small molecular ensembles, thus providing ameliorated conditions for molecular tracking at intracellular level.

In the present paper we present a workflow based on different optical techniques optimized for tracking analysis at cellular and molecular level providing the optimal balance between the required spatial, temporal, and statistical resolution. We developed a highly robotized fluorescence microscopy protocol for the acquisition and analysis of data to characterize the motility of cell populations under different biological conditions. A computer-driven fluorescence microscope has been employed to retrieve information about cell motion and morphology with high statistical significance. To elaborate the relevant amount of collected images, a fully automatic analysis procedure has been developed, able to reconstruct cell dynamics providing single-cell tracks, mean distance, and speed. Correlation of cell motility and morphology changes is performed in order to identify specific phenotypes related to altered migratory properties.

At the same time we show a different tracking procedure based on photoprinting techniques to characterize the intracellular mobility of the molecule responsible of the analyzed phenotype. We employed nonlinear microscopy to achieve real three-dimensional optical confinement, thus uncovering molecular fluxes between different cell compartments.

We discuss the potential of the presented approach to analyze the phenotype induced by overexpression of RAB5, a protein commonly known as component of the endocytic machinery able to transduce and redirect molecular signals to act directly on cell migration programs (Palamidessi et al. 2008).

Materials and methods

Cell culture and transfection

HeLa cells were obtained from American Type Culture Collection (ATCC) and grown in Dulbecco's modified Eagle's medium (DMEM; Cambrex) supplemented with 10% South American serum (EuroClone) and 1% L-glutamine

(EuroClone). The cells were transfected with a pEGFP or with an equimolar mixture of pEGFP and pCMVRAB5A expression vector (kindly provided by M. Zerial) using Fugene 6 (Roche) according to manufacturer instructions. One day after transfection, the cells were detached and sparsely replated in a six-well cell culture plate for random migration assays.

For high-resolution FRAP and photoactivation analysis, the cells were plated on 0.17-mm-thick glass coverslips and mounted in a dedicated enclosure chamber (OKOLAB, Naples, Italy).

High-content migration analysis

Data acquisition

Images were recorded on a Scan^R screening system (Olympus Europe, Germany). The system is composed of an Olympus IX81 (Olympus Italy, Milan, Italy) inverted motorized microscope equipped with a cell incubation chamber (OKOLAB, Naples, Italy) for temperature, humidity, and CO_2 control. A motorized stage (Marzhauser, Germany) allowed for browsing over different positions in and over different wells in a six-well cell culture support. A grid of 49 images was acquired from each well containing the various transfectants. An ORCA-ER Cooled charge-coupled device (CCD) digital camera (HAMAMATSU Italy, Milan, Italy) was employed for image acquisition. Green fluorescent protein (GFP) fluorescence and phase-contrast images were sequentially acquired for cell identification and tracking and for monitoring of cell morphology and membrane remodeling, respectively. Cell observation was performed by a 20× long-working-distance objective (NA 0.45) equipped with a correction ring for plastic. Transmitted light illumination was adopted for a contrast-based autofocus and focal shift between phase-contrast and fluorescence images corrected by introducing an appropriate objective focus repositioning before fluorescence signal acquisition. Data were acquired every 20 min over a 24-h period.

Data analysis

Data analysis was performed with an automatic tracking macro written in ImageJ analysis software (W. Rasband, National Institute of Health, Bethesda, USA).

For each acquired stage position, the temporal sequence of the fluorescence channel images was loaded and analyzed. All the data relative to the 49 fields inside a single well were then merged to build the "motion" phenotype related to the selected biological conditions (Ctrl cells versus RAB5 overexpressing cells versus ROCK inhibited cells).

Briefly, the background was initially estimated and subtracted from recorded data. Flat field correction has been implemented to subtract nonspecific fluorescence and to normalize illumination conditions, employing reference images of selected fields not containing cells.

Particle detection was performed by a *k*-means clustering procedure coded in the available plug-in. The clustering into five different levels of intensity for each image granted an optimal compromise to obtain good particle segmentation and recognition of the cell morphology. The optimized threshold was chosen as the lowest clusterized value (thus limiting oversegmentation effects) providing the highest number of detected particles in the field (thus optimizing object recognition). To limit the introduction of artifacts, acceptable ranges of cell size (minimal and maximal size: 200–3,000 pixels) and circularity (circularity = $4\times\pi\times$area/perimeter^2; range 0.1–1.0) were introduced after manual measurement of the typical cell parameters. The collected data were then automatically segmented and the cells were detected, storing centroid coordinates, circularity, and mean fluorescence.

The trajectories were then reconstructed according to the closest-neighbor selection criteria. The positions of the particles contained in two successive temporal frames were compared. Each particle at time $i + 1$ is assigned to the track of the closest object at time i, if the relative distance is less than a selected cutoff (50 pixels, selected after manual reconstruction of ten randomly chosen trajectories). The introduction of the cutoff was necessary to exclude movements of detached particles, and to limit artifacts due to appearance/disappearance of objects in the field of view. In presence of ambiguous situations created by cell division and track crossing, a restrictive choice was then applied. When two cells at time $i + 1$ originated from the same object (i.e., they shared the same closest neighbor), the corresponding track was interrupted at time i, and two new tracks started at $i + 1$. The occurrence of the event was stored in order to quantify the number of critical events. To outline correlations between motion state and morphology, the tracks were also filtered according to the circularity values.

Tracking procedure validation

The automated tracking procedure was validated by analyzing a set of simulated data. A series of temporal sequences of moving particles was simulated according to a code written in ImageJ analysis software macro language. Cell positions at time $i + 1$ were determined by randomly choosing direction and amplitude of the movements along the X- and Y-axis with respect to the initial spatial coordinates at time i. Each spatial shift was limited by a maximal step in each direction. Cells were represented as

ovals of randomly variable size and orientation. Objects reaching the border of the field of view were scattered back by the residual step along each axis. Images were then subjected to a Gaussian blur filter to mimic microscope imaging process.

To simulate mitotic events, a fixed probability was assigned to each cell to undergo division. For each simulated particle, spatial and temporal coordinates and occurrence of mitosis were stored and subsequently compared with the values calculated by analyzing the images with the automated tracking procedure. The comparison of simulated and calculated tracks was repeated over 50 different runs, each composed of 50 time frames, annotating simulated and detected number of particles, number of tracks, number of mitotic events, X and Y residuals, and average track length.

Confocal and two-photon microscopy

Confocal microscopy analysis was performed on a Leica TCS SP2 AOBS confocal microscope equipped with violet (405 nm laser diode), blue (argon, 488 nm), yellow (561 nm, solid-state laser), and red (633 nm, HeNe laser) excitation laser lines. A 63×/1.4 NA oil-immersion objective (HCX PL APO 63× Lbd Bl, Leica Microsystems) was employed for the analysis. An enclosure microscope chamber allowed for temperature control during the live cell imaging studies.

The acquisition conditions were set to preserve cell viability during FRAP, fluorescence loss in photobleaching (FLIP), and photoactivation analysis. A bidirectional scanning has been employed (speed: 800 lines per second) to obtain optimal temporal resolution and minimal photodamage simultaneously. In FRAP experiments, rapid photobleaching was achieved by limiting the scanned area to the region of interest, whereas in FLIP protocol continuous photobleaching was obtained by selecting maximal illumination power in the targeted region of interest (ROI) through acousto-optical tunable filtering (AOTF).

For two-photon fluorescence microscopy, a Chameleon-XR (Coherent) Ti:sapphire laser source was directly coupled to the scanning head of a Leica TCS SP5 AOBS confocal microscope using an infrared port. Two-photon activation was performed by irradiating a specific vesicle at $\lambda = 790$ nm. The pixel dwell time was set to 4.9 μs using an activation average power of 10 mW. Repeated photoactivation pulses were confined to the targeted region to induce photoactivation by an electro-optical modulator (EOM). Imaging of the activated proteins was performed with the 488-nm line of a 20-mW argon-ion laser using a 100× oil NA 1.4 objective HCX PL APO (Leica Microsystems).

Results

Automated microscopy for high-content cell tracking

Cell motion analysis can largely benefit from an increase in content and throughput to reinforce the statistical significance of the provided results. We employed robotized microscopy to collect a relevant amount of data representative of different biological conditions using green fluorescent protein (GFP) as a fluorescent marker to identify target subpopulations. Fluorescence tagging simultaneously provided an efficient tool for automatic cell tracking. We consequently developed a fully automated analysis procedure to remove the limiting steps introduced by time-consuming human-driven data collection and analysis. The protocol has been tested in the analysis of cell migration after overexpression of selected proteins. Before applying the developed procedure to experimental data analysis we validated it by analyzing a set of simulated images as described in the "Materials and methods" section. Table 1 reports the performances of the tracking algorithm calculated over 50 different runs, demonstrating the validity of the developed approach. The number of calculated track interruptions, and consequently the calculated total number of tracks, is higher than the simulated one due to the assumptions

Table 1 Efficiency of the automated tracking procedure tested on simulated data as reported in the "Materials and methods" section

	No. of particles	No. of tracks	No. of interruptions (mitosis)	Track length
Simulated	2,239.55	73.90	24.45	252.24
Calculated	2,238.39	79.24	27.10	223.78
Simulated − Calculated (%) Mean ± SEM	0.052 ± 0.007	−7.25 ± 0.50	−10.89 ± 0.77	11.29 ± 0.44
$((X_{sim} - X_{cal})^2 - (Y_{sim} - Y_{cal})^2)^{1/2}$ Number of calculated particles (pixels) Mean ± standard error of mean (SEM)	0.00197 ± 0.00016			

The reported values are the average over 50 different simulation runs (50 time frames per run)

adopted in the trajectory reconstruction. If the closest neighbor between successive time frames cannot be uniquely attributed to a single object the corresponding track is interrupted and two or more new trajectories initiated. The occurrence of this event is related to both cell division (two newborn cells lying in proximity of the mother cell) and trajectory intersection, when the criteria of the closest neighbor between two time points loses validity. The automated tracking algorithm detects both of these events, explaining why a higher number of calculated tracks is therefore expected.

The overexpression of RAB5 protein in HeLa human carcinoma cell line induces a dramatic reshaping, characterized by cell body elongation (Fig. 1, panel 1, A–D). Strikingly a similar phenotype can be created by Y27632 drug treatment (Fig. 1, panel 1, E, F), which abolishes blebbing-like movements of amoeboid motility in three-dimensional (3D) migration, interfering with actomyosin contractility dependent on the Rho-ROCK molecular pathway (Sahai and Marshall 2002, 2003). The resulting effect is the establishment of mesenchymal-type motion characterized by the formation of cell protrusions. The molecular activity of RAB5 and its ability to act as a relevant player on actin cytoskeleton remodeling by direct redistribution of RAC (ras-related C3 botulinum toxin substrate) has been recently reported (Lanzetti et al. 2004; Palamidessi et al. 2008).

We employed the developed high-content random-migration assay based on automated fluorescence microscopy to correlate the modifications in cell morphology to an altered motility. The automated image analysis procedure (Fig. 1, panel 2) was designed to identify cells by fluorescence intensity segmentation, performing the measurements required to reconstruct spatiotemporal trajectories. The spatial clustering of fluorescent cells can represent a relevant obstacle in the correct cell recognition. We consequently tested different computational approaches to maximize single-cell discrimination, and adopted a solution based on a *k*-means clustering analysis that allowed the simultaneous optimization of object recognition and morphology measurement capability. Due to the large amount of collected data, stringent conditions to avoid the inclusion of cell aggregates have been selected as described in the "Materials and methods" section. The measurement of the circularity parameter has been chosen to monitor changes in the cell shape. Trajectory reconstitution has been based on the closest-neighbor criteria applied to consecutive time frames. Trajectory intersection and/or ambiguous identification of cell neighbors were considered condition for trajectory interruption. In this way we obtained quite a good rate of exclusion of mitosis-related movements which could potentially introduce artifacts in the analysis. Even though the experimental conditions were set to maximize cell

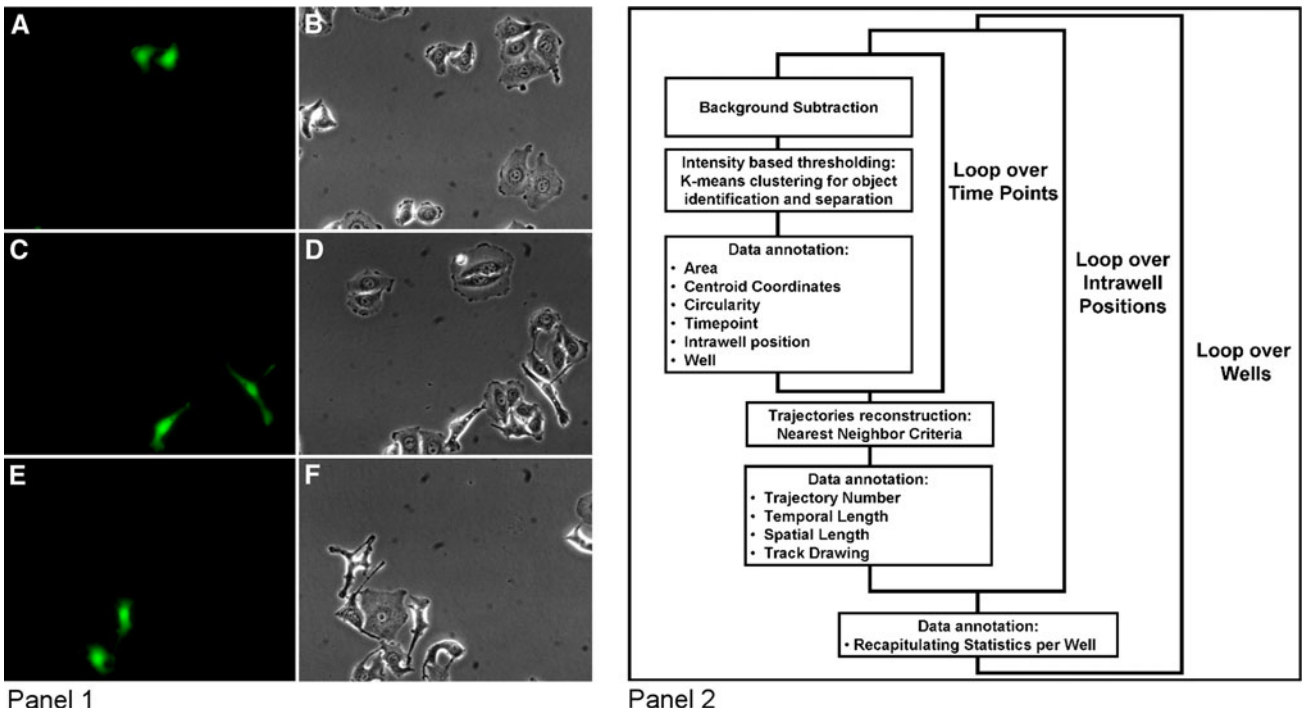

Fig. 1 **Panel 1** RAB5 overexpression-induced morphological changes. HeLa cells were transfected with GFP (*A*,*B*,*E*,*F*) or GFP and RAB5 (*C*,*D*), treated with the Y27632 ROCK inhibitor (*E*,*F*) and analyzed by high-content live cell microscopy. Fluorescence (*column 1*) was employed to target cells for migration measurements. Phase-contrast images (*column 2*) revealed the dramatic reshaping with cell body elongation induced by RAB5 overexpression (*D*) resembling effects of Rho-ROCK pathway inhibition (*E*). **Panel 2** Workflow of the automatic image analysis procedure. See text for details

Table 2 Statistics of the calculated trajectories for Ctrl, ROCK-inhibited (iROCK), and RAB5-overexpressing HeLa cells

	Ctrl	iROCK	RAB5
No. of tracks	404	629	601
No. of detected particles	8,939	12,500	11,926
% of tracks interrupted for mitotic events	3.71	3.50	2.33
% of tracks interrupted for other events	41.83	45.15	40.93

motility over cell division, the biological properties of the adopted cell model and the long time interval monitored (24 h) make the rate of mitotic events not completely negligible. More than 8,500 cells were evaluated for each condition, and more than 400 trajectories were calculated. The developed software is able to superimpose the calculated cell trajectories on the collected movies. We consequently analyzed the interrupted trajectories to verify the real biological event leading to the end of the track. As already mentioned in the data analysis paragraph in the "Materials and methods" section, an ambiguous attribution of the closest event to a single trajectory leads to its interruption and starting of two or more new tracks. This event is imputable to many particles sharing the same spatiotemporal origin. The result reported in Table 2 evidenced that, besides real mitotic events, trajectory interruption can be frequently attributed to variation in the cell number due to variable efficiency in particle identification and separation and to appearance/disappearance of objects into/from the field of view. In particular the high percentages of interrupted track can be mostly imputed to particles escaping from the imaged area.

Spatiotemporal trajectories of the three analyzed cell populations are shown in Fig. 2. All the tracks were spatially normalized to their initial point in order to emanate from the origin of the reference system. It is therefore evident that RAB5-overexpressing cells presented increased cell motility with respect to wild-type cells, as outlined by the larger extension covered by red trajectories. A comparison between RAB5-overexpressing and ROCK-inhibited cell tracks (red and green lines, respectively) showed that the two conditions shared not only similar effects on the reshaping of cells but also superimposable motility-related phenotypes, extending previously published observations (Palamidessi et al. 2008). To quantify cell reshaping due to RAB5 overexpression, cell circularity values were considered: in the wild-type population only 43% of the analyzed objects presented a circularity of less than 0.7 (arbitrary set value), in comparison with 60% of cells with increased RAB5 content. Rock chemical inhibition led to similar percentages (65%).

The distribution of the average displacement (Fig. 3) confirmed the enhanced motility in RAB5-overexpressing cells, showing a shifted modal peak and increased frequencies at high distances.

Finally, to evidence the correlation between the morphological changes induced by RAB5 and altered cell motion, we filtered the trajectories according to the shape detected at single time intervals (20 min). As shown in Fig. 2, panel B, the isolation of motion steps characterized by elongated shape (circularity <0.7) caused a marked disappearance of wild-type cells from the graph, confirming that the RAB5 overexpression induced mesenchymal-like motility in HeLa cells, recapitulating the phenotype induced by Rho-ROCK inhibition.

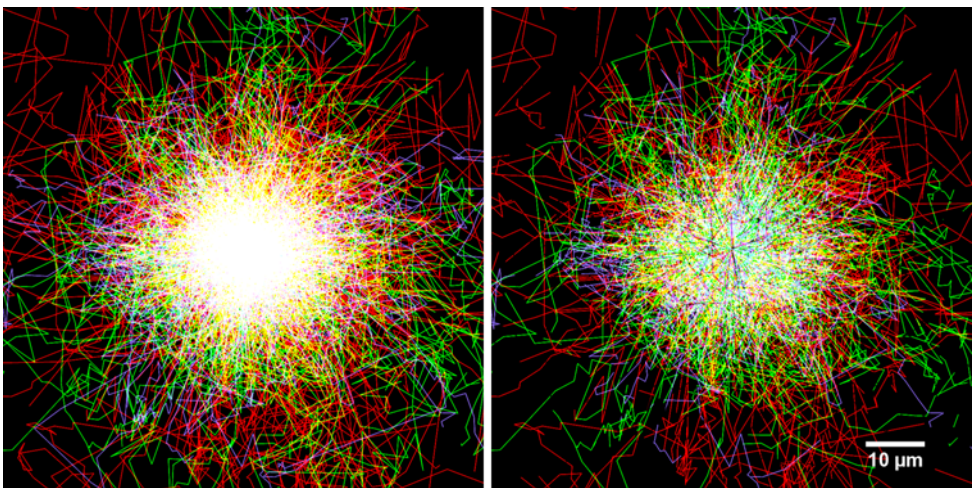

Fig. 2 High-content trajectory reconstruction. Calculated tracks for GFP-transfected (*violet line*), GFP- and RAB5-transfected (*red line*), and GFP-transfected and Y27632-inhibitor-treated (*green line*) HeLa cells are shown in a "spider" graph (starting point translated to the origin of the reference system). About 200 tracks per cell populations are plotted in A. Panel B shows the same graph filtered according to cell shape parameters: only steps characterized by a circularity value of less than 0.7 (arbitrarily fixed) were plotted, emphasizing the "mesenchymal" phenotype induced by RAB5 overexpression and Rho-ROCK pathway inhibition

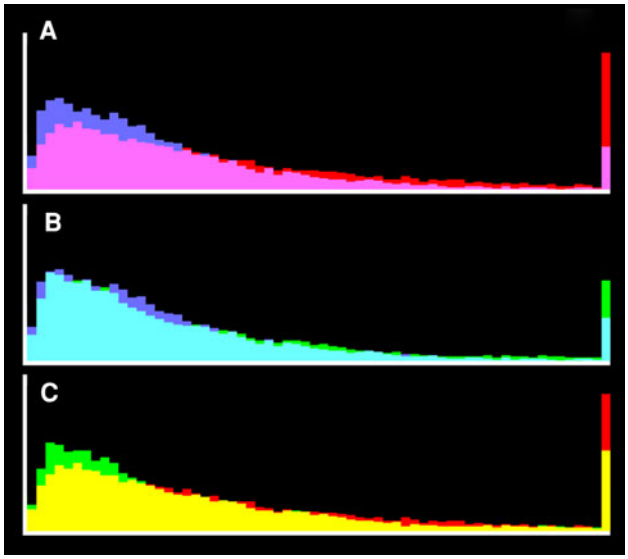

Fig. 3 Average displacement distribution. Average displacement distribution (mean displacement from the trajectory origin) for the three biological conditions were calculated for each time point and plotted. The comparison of Ctrl- and RAB5-overexpressing cells (*A*) revealed an increase after RAB5 overexpression further emphasizing the enhanced mobility acquired. A similar shift was observed following inhibition of the Rho-ROCK pathway (*B*) with comparable effects (*C*) to RAB5 overexpression. Values up to 40 μm were subdivided into 64 frequency classes

Analysis of intracellular molecular fluxes in living cells

The comprehension of the molecular basis of cell migration requires rescaling from cellular to molecular resolution and development of ad hoc tracking algorithms (Kim et al. 2006; Leake et al. 2008). At this level, direct tracking of intracellular objects becomes hard due to the limitations imposed by high-resolution live cell imaging analysis. At the high frame rate required and with the moderate employed power to limit cell photodamage, the signal-to-noise ratio cannot always be fully maximized and conditions avoiding molecular crowding are not easily achieved. The reconstruction of molecular fluxes is thus better achieved by light manipulation to target small ensembles of molecules as in FRAP techniques.

The enhanced cell motility and reshaping observed upon RAB5 overexpression was accompanied by a dramatic actin cytoskeleton remodeling activity (Fig. 4). RAB5 overexpression induced the formation of enlarged endosomes where the actin remodeling enzyme RAC is accumulated (Fig. 4 and Palamidessi et al. 2008). We applied FRAP analysis to characterize the dynamical properties of RAC localization. Targeted photobleaching of GFP-RAC fusion protein revealed that the accumulation of the actin remodeling enzyme on the surface of enlarged endosomes is highly dynamic. The representative time sequence and graph reported in Fig. 5 show that the mobile fraction of molecules approaches 80% of the bleached population (77.06 ± 1.12% standard error, SE) with an average recovery half-time of 2.72 s, thus underlying the presence of remarkable molecular fluxes.

However, FRAP analysis cannot provide information on the directionality of the movements between the compartments. Activated RAC normally resides on cell membrane, where it drives actin remodeling to induce ruffle formation. The aforementioned data demonstrated that RAC is also accumulated in the endocytic compartment and that all the molecules possess an extremely high degree of mobility, but no information could be inferred on the tracks linking the two compartments.

The evaluation of directed molecular fluxes is better achieved by fluorescence loss in photobleaching protocols. Continuous photobleaching of a region of interest allows highlighting of molecular exchanges by monitoring the

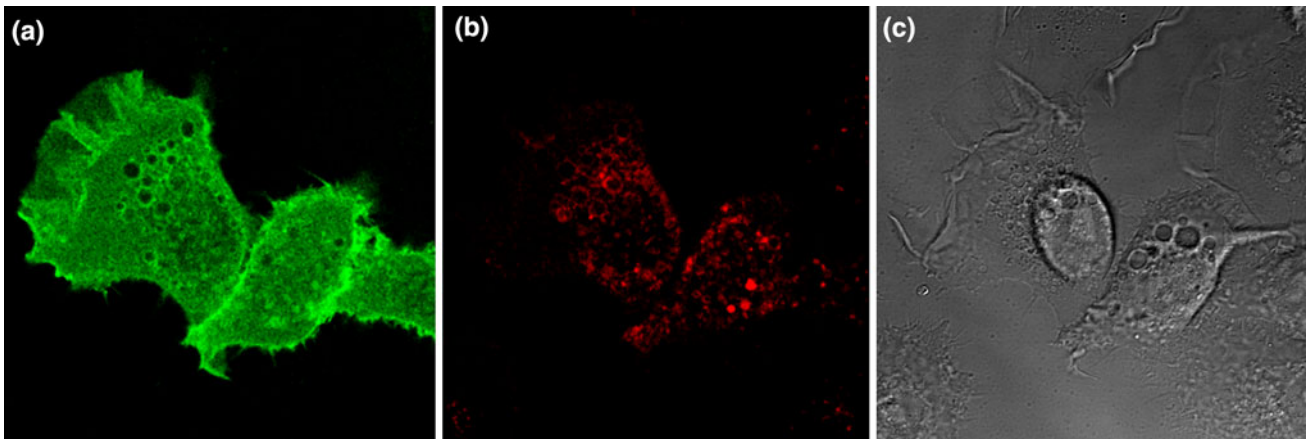

Fig. 4 High-resolution analysis of RAB5 overexpression in living cells. Confocal microscopy analysis of RAB5-transfected cells. The cells were cotransfected with a RAC-GFP construct (**a**) to monitor actin cytoskeleton remodeling, and incubated with tetramethylrhodamine isothiocyanate (TRITC)-conjugated transferrin (**b**) to identify the endocytic compartment

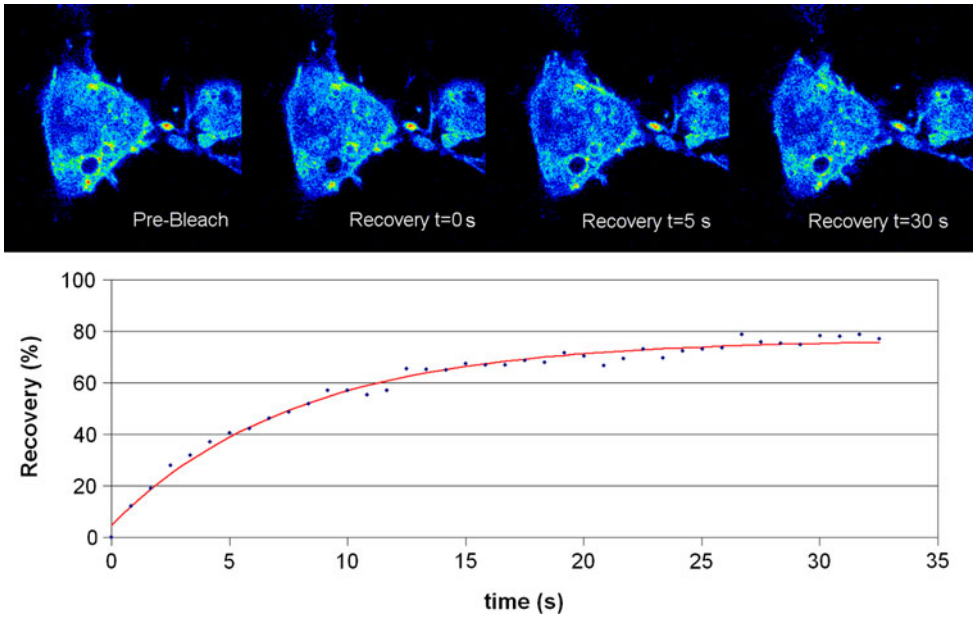

Fig. 5 Analysis of RAC mobility by fluorescence recovery after photobleaching. The dynamics of RAC-GFP accumulated in enlarged endosomes was evaluated by targeted photobleaching of the endocytic compartment. The rapid recovery showed a high turnover of the protein. The measured fluorescence recovery was fitted by a single exponential model: $a(1 - \exp(-bt)) + c$ (*red line* in the graph)

temporal evolution of the fluorescence intensity in external areas: if a direct communication between the compartments exists, the relocalization of bleached molecules will cause a progressive reduction in the measured values.

To evaluate the presence of directed RAC fluxes originating from the plasma membrane towards enlarged endosomes, we consequently applied a FLIP protocol targeting a peripheral region of the cell with high-power laser illumination. The same conditions were simultaneously applied to induce photobleaching of TRITC-conjugated transferrin, a molecular marker of endocytic vesicles. The continuous photobleaching of GFP-RAC caused progressive reduction in fluorescence over the entire cell (Fig. 6), emphasizing the existence of fluxes connecting plasma membrane and enlarged endosomes through the cell cytoplasm. On the contrary, photobleaching of plasma membrane regions did not affect transferrin fluorescence intensity in the pre-existing endocytic compartment. This observation is in agreement with the notion that transferrin is directed to routes leading to endosome degradation and recycling to the plasma membrane, but over a longer time scale.

The extension of the illumination cone of the Gaussian laser beam of a confocal microscope does not allow real three-dimensional control of the targeted region. Both in-focus and out-of-focus planes are illuminated simultaneously. Consequently the question of whether a reverse flux of RAC molecules recycled from the endocytic compartment to the plasma membrane exists cannot be addressed with conventional FRAP techniques. Even though high-power illumination can be confined to single endosomes in the focal plane, the corresponding sections of basal and apical plasma membrane lying on the optical axis are inevitably subjected to a relevant photon rate, thus experiencing uncontrolled photobleaching.

Two-photon excitation possesses an intrinsic optical confinement limiting excitation to a small volume around the focal plane. Outer sections are consequently unaffected by illumination. In some recent works we demonstrated that nonlinear light absorption can be employed to induce photoconversion of specific fluorescent molecules with switchable photophysical properties such as photoactivatable green fluorescent protein (paGFP) (Diaspro et al. 2006; Testa et al. 2008a, b). paGFP is essentially nonfluorescent in its native form when illuminated with blue light (normally employed to excite GFP). However exposure to short high-energy pulses of violet radiation at 405 nm or at selected wavelengths in the infrared (IR) spectral range causes a dramatic alteration in its absorption spectra, thus producing a bright fluorescence upon 488-nm light absorption. In this way photoactivation can be employed to highlight molecules to track their motion over time. The advantage created by the possibility to follow a fluorescent signal over dark background makes photoactivation a more powerful tool in comparison to FRAP-based techniques to target small ensembles of molecules.

Direct tracking of diffraction-limited objects is a challenging task in terms of the temporal resolution of the event and the high fluorescence background created by unbound molecules. The ability to highlight a small fluorescent subpopulation now makes tracking feasible, creating a tool complementary to direct tracking of molecules that can sometimes be employed as an alternative when the number of targeted objects can be maintained low.

We consequently produced a RAC-paGFP fusion protein to underscore potential recycling originated from

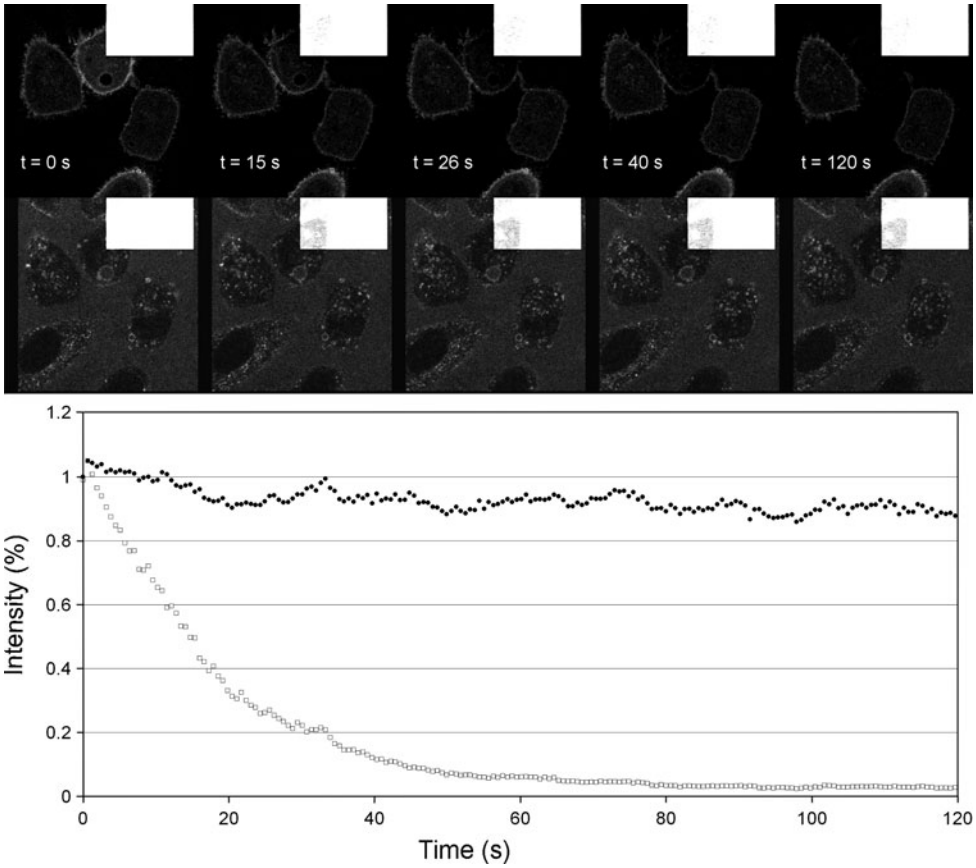

Fig. 6 Fluorescence loss in photobleaching for the monitoring of molecular fluxes. The exchange of molecules from the plasma membrane to the endocytic compartment was monitored by continuous photobleaching of a targeted membrane region (*highlighted pixels* in the images). Temporal monitoring of the fluorescence intensity of RAC-GFP (*first row* and *open squares* in the graph) and TRITC-transferrin (*second row* and *black dots* in the graph) revealed the different dynamical nature of the localization of the two proteins in the endocytic compartment. The measurements were normalized to their initial value. The negligible slope of the transferrin curve reflects a minimal photobleaching due to the imaging conditions and focal-plane variability

endosomes and redirected to the plasma membrane. The two-photon laser source power was calibrated in order to confine the photoactivating pulse to the volume of single vesicles. As shown in Fig. 7, repeated illumination of the targeted vesicle gave rise to a temporally shifted increase in fluorescence in different regions of the plasma membrane. Activated RAC-paGFP molecules moved from the enlarged endosome of origin to the plasma membrane, traveling through the cytoplasm, demonstrating the existence of a reversed molecular flux opposed to the one observed by the FLIP technique on the membrane–endocytic compartment route.

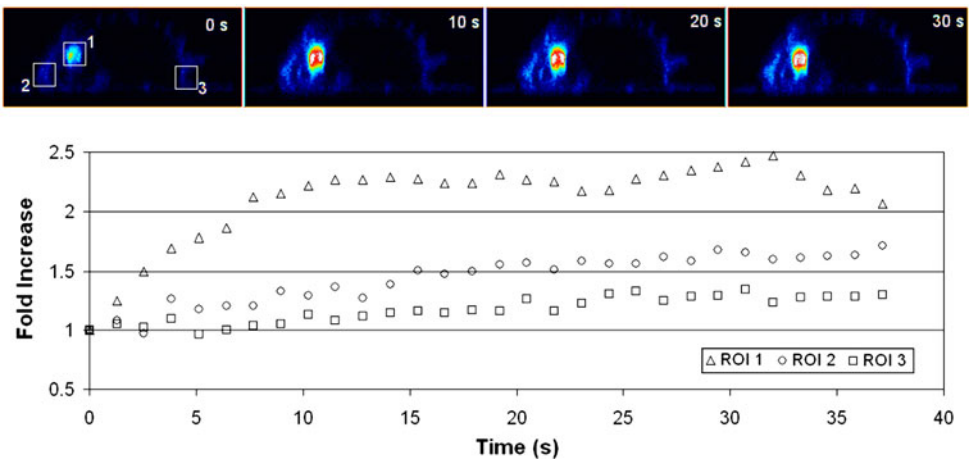

Fig. 7 Two-photon induced photoactivation for the measurement of RAC recycling. Nonlinear excitation was employed to obtain a three-dimensionally confined activation of RAC-paGFP molecules present in an enlarged endosomes. The depicted regions in the first *XZ* section (time 0) delineate the targeted area for photoactivation (area 1) and two membrane portions (areas 2 and 3). The increase in fluorescence over time (*graph*) in the targeted ROIs uncovers a molecular flux of molecules originating from the endocytic compartment and directed to the plasma membrane

Discussion

The wide variety of requests from biological research calls for the creation of new technologies and continuous adaptation of existing microscopy techniques to optimize the amount and quality of collected data. However, the impossibility of simultaneously maximizing the resolution of all the collected parameters (space, time, signal-to-noise ratio, number of fluorescence signals, fields of view, and number of cells) imposes a careful design of the experimental approach in order to associate the most informative optical tools with the best imaging conditions.

We present herein an experimental workflow for biological tracking, working from cellular to molecular resolution. The developed analysis was consequently employed for the characterization of a specific phenotype involving alterations of the cellular migratory properties and then for the dissection of the mechanistic basis of the observed enhancement in cell motility.

The tracking of cells is frequently limited by low-throughput data acquisition and manual data annotation, which is inherently biased and nonquantitative. These bottlenecks can be removed by developing automation solutions for microscopy. The imaging station presented in this work is able to follow living cells for long time intervals, collecting relevant amount of data (about 1,000 images per hour and a total of about 10,000 cells identified) that can be subsequently processed for the reconstruction of cellular trajectories. Multiparameter analysis allowed the correlation of morphological parameters and migratory properties. The definition of migratory phenotypes is in fact partially based on the recognition of cell reshaping due, for example, to the transition from a mesenchymal, characterized by filopodia extrusion and generally elongated cell morphology, to an amoeboid motility, where the cell body tends to assume a spherical shape. The analytical procedure we developed bases its ability to reconstruct the spatiotemporal evolution of single cells on a nearest-neighbor hypothesis. Under the present experimental conditions, the algorithm demonstrated its robustness thanks to the low cell density typical of assays aimed at measuring random migration and the optimized temporal sampling. To improve this ability we plan to include in the software multiple-parameter scoring for cell recognition, simultaneously taking into account position, fluorescence intensity, and size as distinctive features to identify single cells over time. This implementation will also allow inclusion in the analysis of other relevant biological events such as cell cycle progression. Thanks to the high degree of automation the content of the workflow can be further enhanced by including additional fluorescence channels tagging, for example, DNA, thus providing a direct marker for the monitoring of cell division. As a second improvement we plan to modify the data collection approach to image adjacent fields. The mosaic reconstruction of such an enlarged field of view will reduce the number of trajectory interruptions, making it possible to follow cells migrating out of a single CCD-limited spatial frame.

One present limitation of the system is its intrinsic spatial bidimensionality, linked to wide-field observation. An extension to optical sectioning devices could be particularly helpful both for in vitro (3D migration through Matrigel layers) and in vivo studies. However the aforementioned requirements for an optimal balance between the spatial, temporal, and "statistical" resolution call for new technologies and intensive efforts from the computational point of view. A brilliant example of developments in this direction is represented by a recent publication by Keller et al. (2008), where tracking of cells during zebrafish early embryonic development has been successfully implemented by scanned light-sheet microscopy.

While cell tracking requires extension of the field of view in order to get a statistically relevant number of targeted cells, the reconstruction of molecular movements at intracellular level suffers from decreased resolution in crowding conditions, making conventional GFP tagging unsuitable to this task. Fluorescence manipulation can be consequently employed to tag small molecular ensembles, as shown in the presented FRAP and photoactivation protocols. FRAP is able to highlight the kinetic origin of chemical gradients, and its FLIP variant can successfully uncover the directionality of the molecular fluxes between cell compartments. FRAP is in general an inverse marking technique: the behavior of a fraction of tagged (bleached) molecules is determined by observing redistribution of the untagged (fluorescent) fraction. Photoactivation provides the advantage of direction recognition of the target by following the emitted light of activated molecules over the dark background of proteins in their native form. Resolution increases as the number of activated molecules decreases, thus allowing precise highlighting of small compartments. We showed that the intrinsic optical confinement of nonlinear excitation limiting photoconversion up to femtoliter volume can be successfully employed to determine the recycling of molecules from the endocytic compartment to the plasma membrane.

The combination of the presented optical techniques gave rise to a workflow able to shed light on the molecular fluxes connecting different cell compartments. This provided the basis for the comprehension of the molecular mechanisms regulating the motion-related phenotype initially analyzed, by adapting the correct optical tool to the desired resolution. FRAP demonstrated the dynamic nature of the chemical gradient leading to RAC accumulation on the surface of enlarged endosomes, while fluorescence loss in photobleaching revealed the presence of continuous molecular communication connecting the plasma membrane

and the endosome itself. Finally, the innovative employment of nonlinear excitation to induce photoactivation, thanks to its intrinsic three-dimensional confinement, demonstrated that activated RAC molecules moved back to the plasma membrane.

Optical confinement by alternative techniques such as two-photon microscopy provides new potential developments, which open the way to photomarking techniques in vivo. In this last case, even cellular tracking at low spatial resolution can benefit greatly from the increased penetration depth and limited illumination volume of nonlinear microscopy. The target cells could therefore be highlighted in an environment as complex as an organism and dynamically followed in their migration. Unfortunately, photomanipulation still suffers from a quite low throughput. New automated solutions are desired in the near future in order to achieve a breakthrough in the statistical resolution of tracking protocols based on photoprinting techniques.

Acknowledgments This work was supported by IIT (Italian Institute of Technology, Genoa, Italy) and by IFOM (FIRC Institute of Molecular Oncology, Milan, Italy). The authors are grateful to Dr. Francesca Ballarini for her help in manuscript preparation.

References

Bansal V, Patel S, Saggau P (2006) High-speed addressable confocal microscopy for functional imaging of cellular activity. J Biomed Opt 11:34003. doi:10.1117/1.2209562

Diaspro A, Testa I, Faretta M, Magrassi R, Barozzi S, Parazzoli D, Vicidomini G (2006) 3D localized photoactivation of pa-GFP in living cells using two-photon interactions. Conf Proc IEEE Eng Med Biol Soc 1:389–391

Graf R, Rietdorf J, Zimmermann T (2005) Live cell spinning disk microscopy. Adv Biochem Eng Biotechnol 95:57–75

Hell SW (2007) Far-field optical nanoscopy. Science 316:1153–1158. doi:10.1126/science.1137395

Hell SW (2009) Microscopy and its focal switch. Nat Methods 6:24–32. doi:10.1038/nmeth.1291

Keller PJ, Schmidt AD, Wittbrodt J, Stelzer EH (2008) Reconstruction of zebrafish early embryonic development by scanned light sheet microscopy. Science 322:1065–1069. doi:10.1126/science.1162493

Kim SY, Gitai Z, Kinkhabwala A, Shapiro L, Moerner WE (2006) Single molecules of the bacterial actin MreB undergo directed treadmilling motion in Caulobacter crescentus. Proc Natl Acad Sci USA 103:10929–10934. doi:10.1073/pnas.0604503103

Kurtz R, Fricke M, Kalb J, Tinnefeld P, Sauer M (2006) Application of multiline two-photon microscopy to functional in vivo imaging. J Neurosci Methods 151:276–286. doi:10.1016/j.jneumeth.2005.12.003

Lanzetti L, Palamidessi A, Areces L, Scita G, Di Fiore PP (2004) Rab5 is a signalling GTPase involved in actin remodelling by receptor tyrosine kinases. Nature 429:309–314. doi:10.1038/nature02542

Leake MC, Chandler JH, Wadhams GH, Bai F, Berry RM, Armitage JP (2006) Stoichiometry and turnover in single, functioning membrane protein complexes. Nature 443:355–358. doi:10.1038/nature05135

Leake MC, Greene NP, Godun RM, Granjon T, Buchanan G, Chen S, Berry RM, Palmer T, Berks BC (2008) Variable stoichiometry of the TatA component of the twin-arginine protein transport system observed by in vivo single-molecule imaging. Proc Natl Acad Sci USA 105:15376–15381. doi:10.1073/pnas.0806338105

Lippincott-Schwartz J, Manley S (2009) Putting super-resolution fluorescence microscopy to work. Nat Methods 6:21–23. doi:10.1038/nmeth.f.233

Maddox PS, Moree B, Canman JC, Salmon ED (2003) Spinning disk confocal microscope system for rapid high-resolution, multimode, fluorescence speckle microscopy and green fluorescent protein imaging in living cells. Methods Enzymol 360:597–617. doi:10.1016/S0076-6879(03)60130-8

Palamidessi A, Frittoli E, Garre M, Faretta M, Mione M, Testa I, Diaspro A, Lanzetti L, Scita G, Di Fiore PP (2008) Endocytic trafficking of Rac is required for the spatial restriction of signaling in cell migration. Cell 134:135–147. doi:10.1016/j.cell.2008.05.034

Reddy GD, Saggau P (2005) Fast three-dimensional laser scanning scheme using acousto-optic deflectors. J Biomed Opt 10:064038. doi:10.1117/1.2141504

Saggau P (2006) New methods and uses for fast optical scanning. Curr Opin Neurobiol 16:543–550. doi:10.1016/j.conb.2006.08.011

Sahai E, Marshall CJ (2002) RHO-GTPases and cancer. Nat Rev Cancer 2:133–142. doi:10.1038/nrc725

Sahai E, Marshall CJ (2003) Differing modes of tumour cell invasion have distinct requirements for Rho/ROCK signalling and extracellular proteolysis. Nat Cell Biol 5:711–719. doi:10.1038/ncb1019

Testa I, Garre M, Parazzoli D, Barozzi S, Ponzanelli I, Mazza D, Faretta M, Diaspro A (2008a) Photoactivation of pa-GFP in 3D: optical tools for spatial confinement. Eur Biophys J 37:1219–1227. doi:10.1007/s00249-008-0317-9

Testa I, Parazzoli D, Barozzi S, Garre M, Faretta M, Diaspro A (2008b) Spatial control of pa-GFP photoactivation in living cells. J Microsc 230:48–60. doi:10.1111/j.1365-2818.2008.01951.x

Ulbrich MH, Isacoff EY (2007) Subunit counting in membrane-bound proteins. Nat Methods 4:319–321

Wolleschensky R, Zimmermann B, Kempe M (2006) High-speed confocal fluorescence imaging with a novel line scanning microscope. J Biomed Opt 11:064011. doi:10.1117/1.2402110